3.2. Radiological and histological analyses

Fig. 3 represents radiographs of rabbit femurs 4, 12, 24 and 72 weeks after the operation. At 4 weeks post-surgery, the implanted HHA was recognized clearly by its amorphous radiopacity on X-ray film, and no difference from the finding of SHA was seen (Fig. 3a,e). At 12 weeks, radiopacity derived from HHA was evident, but the margin was a little unclear compared to the finding of SHA (Fig. 3b,f). At 24 weeks, no difference in amorphous radiopacity of the implanted HHA was seen compared to the radiopacity at 12 weeks post-surgery (Fig. 3b,c). In radiographic appearance, the radiopacity of implanted SHA was similar from 2 to 24 weeks after the operation (Fig. 3e–g). Seventy-two weeks after the operation, the area of HHA implantation was not evident (Fig. 3d). The radiopacity of SHA was similar to those in earlier stages, but slight irregularity of the marginal region and enlargement of macropores were seen (Fig. 3h).

Histological analyses were conducted using plastic-embedded undecalcified sections stained for TRAP activity or sections stained with toluidine blue. Two weeks after the implantation of HHA, TRAP-positive osteoclasts were seen on the surface of the implant. Part of the implant directly contacted with bone (Fig. 4a). Four weeks after implantation of HHA, the histological features were similar to those at 2 weeks. Bone tissue in contact with HHA and TRAP-positive cells in contact with HHA were seen (Fig. 4b). Twelve weeks after the operation, the invasion of newly formed bone tissue into HHA implants was evident and many osteoclasts in contact with newly formed bone or HHA were seen (Fig. 4c). Twenty-four weeks after the operation, a considerable amount of HHA remained; however, the amount of newly formed bone invading the implant had increased compared with at 12 weeks (Fig. 4c,d). Infiltration of TRAP-positive osteoclasts was still evident (Fig. 4d). No evidence of bioresorption of the SHA implant was seen from 2 to 24 weeks after the operation (Fig. 5a–d). TRAP-positive osteoclasts were seen on the surface of the implant from 2 to 24 weeks after the operation, but there were fewer than those in contact with HHA.

At 72 weeks post-operation, most HHA was resorbed and substituted with newly formed bone tissue (Fig. 6a). Invasion of bone tissue into the cracked SHA implant was seen in some portions, and TRAP-positive osteoclasts were seen in these regions. Some osteoclasts contacted with SHA, but no evidence of osteoclastic resorption was seen (Fig. 6b).

3.3. Histomorphometry

Histomorphometric quantitation revealed that BV/TV in specimens implanted with HHA was significantly greater than that in specimens implanted with SHA 24 weeks after the operation (Fig. 10a). The fluorescent signal derived from calcein labeling was analyzed using a fluorescence microscope in the specimens 12 and 24 weeks after the implantation of either HHA or SHA. The width of double labeling was greater in specimens implanted with HHA than in those implanted with SHA at 12 weeks post-operation (Figs. 7b

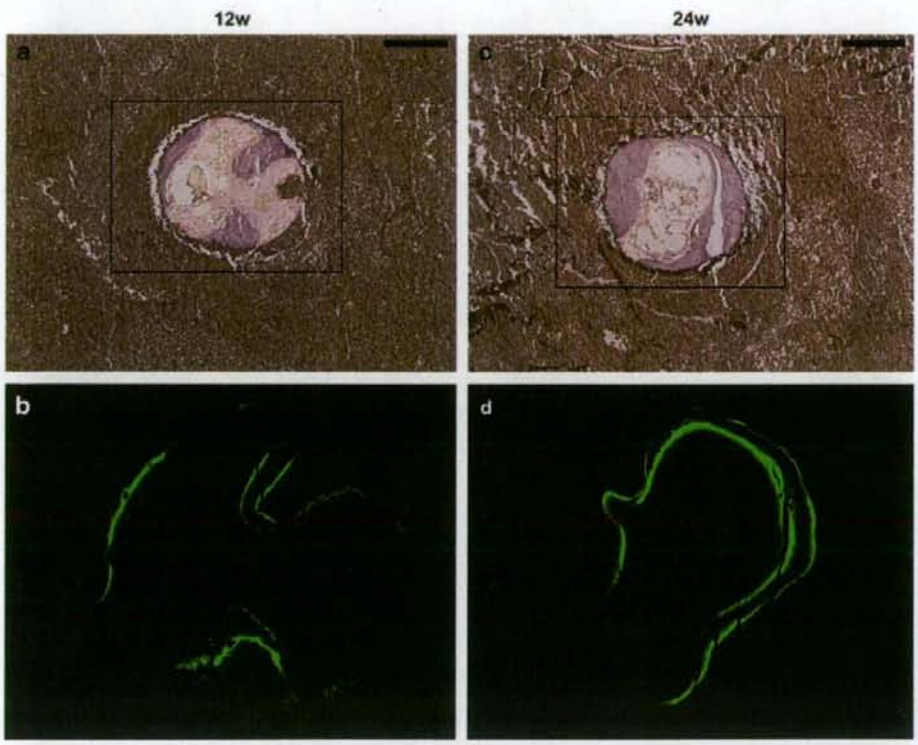

Fig. 8. Evaluation of osteogenesis in a specimen implanted with SHA by fluorescent labeling. (a,c) Bright-field light microscopic appearance of specimens 12 weeks (a) and 24 weeks (c) after SHA implantation. Sections were stained for TRAP activity. The rectangles represent the area used for fluorescent analysis. (b,d) The calcein signal in newly formed bone tissue in the specimens 12 weeks (b) and 24 weeks (d) after SHA implantation. Sections stained with toluidine blue were utilized for analysis by fluorescence microscopy. Bar: (a,c) 100 μm.

and 8b), but was not clear at 24 weeks post-operation (Figs. 7d and 8d). MAR and BFR/BS for newly formed bone tissue in each sample were quantified by histomorphometry. MAR was significantly increased in specimens implanted with HHA in comparison to specimens implanted with SHA at 12 and 24 weeks post-operation (Figs. 9b and 10b). BFR/BS revealed a strong tendency to increase in specimens implanted with HHA as compared with specimens implanted with SHA at 12 and 24 weeks after the operation (Figs. 9c and 10c). Additionally, N.Oc/B.Pm and Oc.S/BS were quantified and both were significantly increased in specimens implanted with HHA compared with those implanted with SHA at 12 and 24 weeks after the operation (Figs. 9d,e and 10d,e).

3.4. In vitro analyses of differentiation of osteoblasts and osteoclasts

Osteoblastic differentiation on HHA and SHA discs was analyzed using C2C12 preosteoblastic cells stimulated with recombinant human BMP-2. When C2C12 cells were cultured in medium supplemented with BMP-2 on an HHA or SHA disc, alkaline phosphatase activity was detected similarly in cells cultured on HHA and SHA discs (Fig. 11a,b). Additionally, mouse bone marrow macrophages were cultured in medium supplemented with recombinant mouse RANKL and M-CSF on discs made with HHA or SHA. Higher TRAP activity was detected in osteoclasts formed on the HHA disc than that in osteoclasts formed on the SHA disc (Fig. 11c,d). To analyze the cause of higher TRAP activity on the HHA disc, the density of cultured cells on the discs was analyzed by nuclear staining with DAPI. The density of DAPI-positive viable nuclei on HHA and SHA discs was similar (Fig. 11e,f).

4. Discussion

In this study, we confirmed that SHA was non-biodegradable in bone tissue. Throughout the experimental period, TRAP-positive osteoclasts were detected on the surface of SHA, but no evidence of osteoclastic resorption was seen (Figs. 5 and 6b). These data suggested that SHA had the potential to be recognized, but was unable to be resorbed by osteoclasts in bone. We previously showed that calcium concentration did not increase at all in the culture media of SHA, in which many osteoclasts were induced by RANKL-expressing cells [4]. Previous data also suggested that osteoclasts could not resorb SHA.

We showed that HHA had been well-recognized by osteoclasts for a long period after implantation, and mild biodegradability and good substitution for newly formed bone were detected in animal experiments. Previously, calcium-deficient HA was introduced in biological analyses [19], but the XRD pattern was not shown and the purity and uniformity of the material were uncertain. XRD of HHA showed that HHA was pure calcium-deficient HA (Fig. 1) and was composed of uniform rod-shaped particles (Fig. 2). Biodegradation of HHA by osteoclasts during the experimental period showed that molar ratio of Ca/P directly affected osteoclast activity, even though the organic components in bone tissue might also affect osteoclast activity. Biodegradation of HHA was very slow (Fig. 4), but most part of HHA was replaced by newly formed bone up to 72 weeks

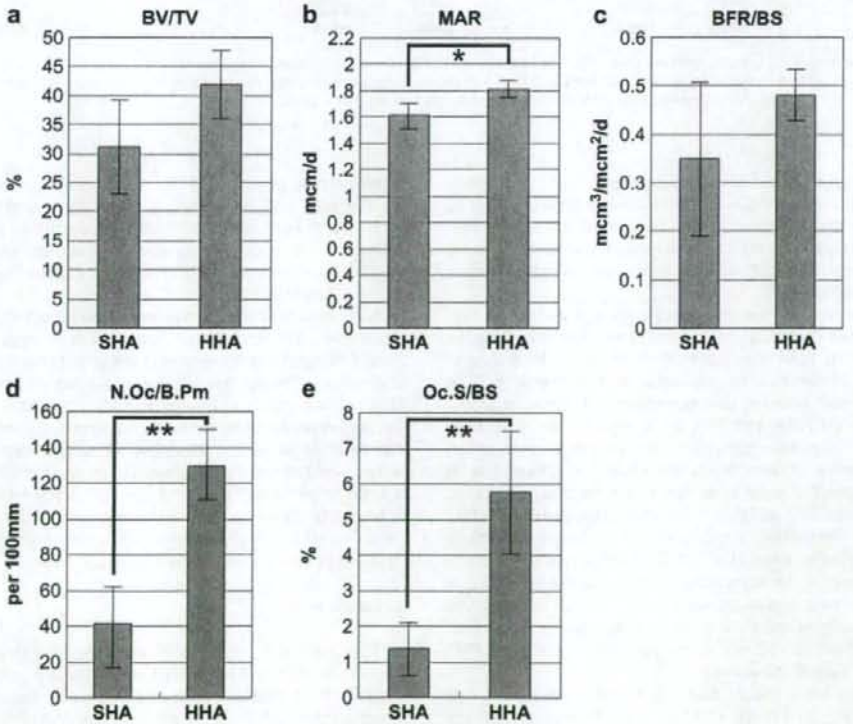

Fig. 9. Histomorphometry of newly formed bone tissue in the specimens 12 weeks after implantation. Parameters for the amount of bone, BV/TV (a), osteogenic activity, MAR (b) and BFR/BS (c), were compared between specimens implanted with HHA and specimens implanted with SHA. Parameters for bone resorption, N.Oc/B.Pm (d) and Oc.S/BS (e) were also compared (*$P < 0.05$, **$P < 0.01$). Three areas in the four samples were analyzed for the data acquired.

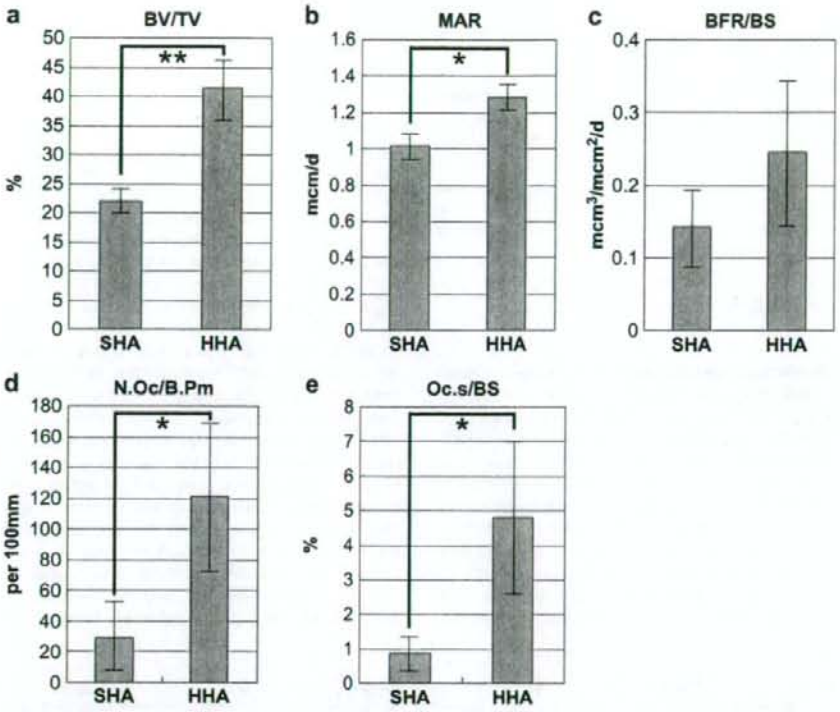

Fig. 10. Histomorphometry of the newly formed bone tissue in the specimens 24 weeks after implantation. Parameters for the amount of bone, BV/TV (a), osteogenic activity, MAR (b) and BFR/BS (c), were compared between specimens implanted with HHA and specimens implanted with SHA. Parameters for bone resorption, N.Oc/B.Pm (d) and Oc.S/BS (e) were also compared (*$P < 0.05$, **$P < 0.01$). Three areas in the four samples were analyzed for the data acquired.

after implantation (Fig. 6a). These data suggested that the solubility of bone substitute did not always correlated to replaceability by bone tissue. We hypothesized that if a bone substitute was continuously recognized and resorbed by osteoclasts, continuous resorption would lead to replacement by new bone tissue irrespective of the mild solubility.

Osteoblast activity in the implanted region of HHA was suggested to be higher than that of SHA from histomorphometric data, which showed that MAR was significantly higher in HHA than in SHA at 12 and 24 weeks after implantation. Considered with in vitro studies, which showed that osteoblastic differentiation occurred similarly on HHA and SHA discs, excess bone formation found in animals implanted with HHA was thought to be caused by indirect stimulation of osteoblasts by HHA. Bone formation is thought to be coupled with bone resorption in that osteoblasts express one of the key molecules for osteoclastogenesis, RANKL [20]. Conversely, the biological mechanism to stimulate osteoblasts by osteoclasts remains uncertain, but the biodegradable nature of HHA was suggested to be associated with the excess bone formation found in animals implanted with HHA. In vitro study showed higher TRAP activity of osteoclasts on HHA than that of osteoclasts on SHA, and active osteoclasts in animals implanted with HHA might influence osteoblast activity.

Previously, we have shown that the microstructure of β-TCP affected the biological response [4,21]. It is conceivable that the microstructure of HA also affects the biological response. As shown in Fig. 2a, HHA was formed by rod-shaped particles just like β-TCP composed of rod-shaped particles, which was prepared by applied hydrothermal process. β-TCP composed of rod-shaped particles showed mild and stable degradability compared to conventional β-TCP composed of globular-shaped particles, and rod-shaped particles were suggested to affect the activity of bone cells and metabolism of subsequently formed bone tissue [4]. This might also be the case in HHA.

Additionally, HHA is composed of hexagonal monocrystals with prolonged *c*-axis and the surface of HHA is suggested to be electrically charged. Previous reports suggested that the surface charge of ceramics affected the affinity or activity of bone cells [22,23]. Although the surface charge of HHA has not been directly measured yet, preferential affinity for acidic protein compared to basic protein was detected at pH 7.2 using bovine serum albumin as an acidic protein and lysozyme chloride as a basic protein [24]. Acidic protein is negatively charged in neutral conditions, and HHA was suggested to be positively charged from the experiments. Surface charge derived from the microstructure of HHA and/or attached proteins on HHA might also influence the biological behavior.

5. Conclusion

The biological response of hydrothermally synthesized pure calcium-deficient HA composed of rod-shaped particles (HHA) was different from that of stoichiometric HA synthesized by the sintering method (SHA). HHA but not SHA revealed a biodegradable nature by osteoclastic resorption. Irrespective of mild biodegradation, HHA showed good replaceability with bone tissue. Excess bone formation found in animals implanted with HHA

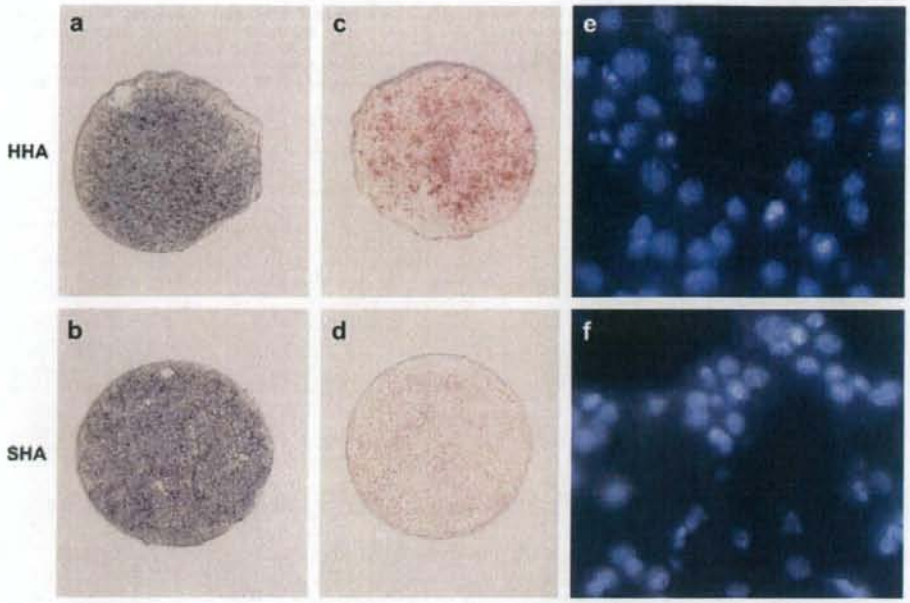

Fig. 11. The in vitro induction assay of osteoblasts and osteoclasts on HHA and SHA discs. (a,b) Alkaline phosphatase-positive C2C12 cells on HHA (a) and SHA (b) discs. (c,d) TRAP-positive bone marrow macrophages induced by recombinant RANKL on HHA (c) and SHA (d) discs. (e,f) Nuclear appearances of bone marrow macrophages cultured on HHA (e) and SHA (f) discs stained with DAPI.

compared with those implanted with SHA was suggested to be associated with the biodegradability of HHA. The method to synthesize biodegradable pure calcium-deficient HA is expected to contribute to developing new biodegradable bone substitutes with adequate biodegradability and bone replaceability.

Acknowledgments

We thank Drs. T. Sawase and D. Ono of the Department of Fixed Prosthodontics and Oral Rehabilitation, Nagasaki University Graduate School of Biomedical Sciences for technical assistance and discussion, and Mr. Takaharu Tsukada of the Department of Experimental Surgery and Biomedical Resources, Juntendo University School of Medicine and Kitayama Labes Co. Ltd. for technical consultations on the animal experiments. This work was supported by a Grant-in-Aid from the ministry of Education, Culture, Sports, Science, and Technology of Japan (Grant nos. 18390519 and 18659541) and "Ground-based Research Program for Space Utilization" promoted by Japan Space Forum.

References

[1] Toya H, Ito A, Fujimori H, Goto S, Ioku K. In vitro estimation of calcium phosphate with pH-controlled simulated body fluid. Trans Mater Res Soc Jpn 2001;26:1247–50.
[2] Ioku K, Misumi H, Fujimori H, Goto S. Porous β-tricalcium phosphate ceramics of bimodal pore size distribution. Trans Mater Res Soc Jpn 2003;28:781–4.
[3] Ioku K, Kawachi G, Nakahara K, Ishida EH, Minagi H, Okuda T, et al. Porous granules of β-tricalcium phosphate composed of rod-shaped particles. Key Eng Mater 2006;309–311:1059–62.
[4] Okuda T, Ioku K, Yonezawa I, Minagi H, Kawachi G, Gonda Y, et al. The effect of the microstructure of β-tricalcium phosphate on the metabolism of subsequently formed bone tissue. Biomaterials 2007;28:2612–21.
[5] Bucholz RW, Carlton A, Holmes R. Interporous hydroxyapatite as a bone graft substitute in tibial plateau fractures. Clin Orthop Relat Res 1989;240:53–62.
[6] Hoogendoorn HA, Renooij W, Akkermans LM, Visser W, Wittebol P. Long-term study of large ceramic implants (porous hydroxyapatite) in dog femora. Clin Orthop Relat Res 1984;187:281–8.
[7] LeGeros RZ. Properties of osteoconductive biomaterials: calcium phosphates. Clin Orthop Relat Res 2002;395:81–98.
[8] LeGeros R. Biological and synthetic apatite. In: Broen PW, Constaqntz B, editors. Hydroxyapatite and related materials. CRC Press; 1994. p. 3–28.
[9] Kim HM, Rey C, Glimcher MJ. Isolation of calcium-phosphate crystals of bone by non-aqueous methods at low temperature. J Bone Miner Res 1995;10:1589–601.
[10] Ioku K, Kawachi G, Yamasaki M, Toda H, Fujimori H, Goto S. Hydrothermal preparation of porous hydroxyapatite with tailrod crystal surface. Key Eng Mater 2005;288–289:521–4.
[11] Ioku K, Kawachi G, Sasaki S, Fujimori H, Goto S. Hydrothermal preparation of tailrod hydroxyapatite. J Mater Sci 2006;41:1341–4.
[12] Yoshimura M, Suda H, Okamoto K, Ioku K. Hydrothermal synthesis of biocompatible whiskers. J Mater Sci 1994;29:3399–402.
[13] Ioku K, Nishimura S, Eguchi Y, Goto S. Hydrothermal preparation of porous hydroxyapatite ceramics. Rev High Pressure Sci Technol 1998;7:1398–400.
[14] Ioku K, Misumi H, Fujimori H, Goto S, Yoshimura M. Porous ceramics of calcium phosphates prepared by hydrothermal method. In: Re R, editor. Proceedings of the 5th international conference on solvo-thermal reactions, 2002, USA; 2002. p. 233–6.
[15] Ikeda T, Kasai M, Suzuki J, Kuroyama H, Seki S, Utsuyama M, et al. Multimerization of the receptor activator of nuclear factor-kappaB ligand (RANKL) isoforms and regulation of osteoclastogenesis. J Biol Chem 2003 Nov 21;278(47):47217–22.
[16] Parfitt AM, Drezner MK, Glorieux FH, Kanis JA, Malluche H, Meunier PJ, et al. Bone histomorphometry: standardization of nomenclature, symbols, and units. Report of the ASBMR Histomorphometry Nomenclature Committee. J Bone Miner Res 1987;2:595–610.
[17] Zhao B, Katagiri T, Toyoda H, Takada T, Yanai T, Fukuda T, et al. Heparin potentiates the in vivo ectopic bone formation induced by bone morphogenetic protein-2. J Biol Chem 2006;281:23246–53.
[18] Suzuki J, Ikeda T, Kuroyama H, Seki S, Kasai M, Utsuyama M, et al. Regulation of osteoclastogenesis by three human RANKL isoforms expressed in NIH3T3 cells. Biochem Biophys Res Commun 2004;314:1021–7.
[19] Kasten P, Vogel J, Luginbuhl R, Niemeyer P, Tonak M, Lorenz H, et al. Ectopic bone formation associated with mesenchymal stem cells in a resorbable calcium deficient hydroxyapatite carrier. Biomaterials 2005;26:5879–89.
[20] Suda T, Takahashi N, Udagawa N, Jimi E, Gillespie MT, Martin TJ. Modulation of osteoclast differentiation and function by the new members of the tumor necrosis factor receptor and ligand families. Endocr Rev 1999;20:345–57.

[21] Yokozeki H, Hayashi T, Nakagawa T, Kurosawa H, Shibuya K, Ioku K. Influence of surface microstructure on the reaction of the active ceramics in vivo. J Mater Sci Mater Med 1998;9:381–4.
[22] Nakamura S, Kobayashi T, Yamashita K. Numerical osteobonding evaluation of electrically polarized hydroxyapatite ceramics. J Biomed Mater Res A 2004; 68:90–4.
[23] Itoh S, Nakamura S, Kobayashi T, Shinomiya K, Yamashita K, Itoh S. Effect of electrical polarization of hydroxyapatite ceramics on new bone formation. Calcif Tissue Int 2006;78:133–42.
[24] Kawachi G, Sasaki S, Nakahara K, Ishida EH, Ioku K. Porous apatite carrier prepared by hydrothermal method. Key Eng Mater 2006;309–311: 935–8.

Osteoconductivity of hydrothermally synthesized beta-tricalcium phosphate composed of rod-shaped particles under mechanical unloading

Yoshinori Gonda[1, 2, a], Koji Ioku[3, b], Takatoshi Okuda[2, c], Yasuaki Shibata[1, d], Masanobu Kamitakahara[3, e], Giichiro Kawachi[4, f], Ikuho Yonezawa[2, g], Hisashi Kurosawa[2, h] and Tohru Ikeda[1, i]

[1]Division of Oral Pathology and Bone Metabolism, Department of Developmental and Reconstructive Medicine, Nagasaki University Graduate School of Biomedical Sciences, 1-7-1 Sakamoto, Nagasaki 852-8588, Japan

[2]Department of Orthopedic Surgery, School of Medicine, Juntendo University, 2-1-1 Hongo, Tokyo 113-8421, Japan

[3]Graduate School of Environmental Studies, Tohoku University, 6-6-20Aramaki, Aoba-ku, Sendai 980-8579, Japan

[4]Department of Crystalline Materials Science, Graduate School of Engineering, Nagoya University, Furo-cyo, Chikusa-ku, Nagoya 464-8603, Japan

[a]gondayoshinori@mac.com, [b]ioku@mail.kankyo.tohoku.ac.jp, [c]o-kun@med.juntendo.ac.jp, [d]siva@nagasaki-u.ac.jp, [e]kamitaka@mail.kankyo.tohoku.ac.jp, [f]kawachi@apchem.nagoya-u.ac.jp, [g]yoza@med.juntendo.ac.jp, [h]kuro@med.juntendo.ac.jp, [i]tohrupth@net.nagasaki-u.ac.jp

Keywords: Beta tricalcium phosphate, Bone graft, Unloading

Abstract. Spherical beta-tricalcium phosphate (β-TCP) granules synthesized using a unique dropping slurry method expressed good osteoconductivity with prominent bone apposition and bioresorbability when implanted into the rat femur (Gonda et al., *Key Eng. Mater.* 361-363:1013-1016, 2008). The spherical β-TCP granules were implanted into the bone defect created in the distal end of the right femur of each 8-week-old female Wistar rat. To analyze performance of the spherical β-TCP granules as bone substitute in the bone with reduction in osteogenic potential, the right sciatic neurectomy was performed after implantation and the right hind limb was kept unloaded for 2 weeks before euthanization. Four weeks after implantation, some spherical β-TCP granules with resorption in part were surrounded by newly formed bone. Eight and 12 weeks after implantation, most of the residual β-TCP granules were embedded in newly formed bone, and total volume of the implant and newly formed bone was more than the other portions of the bone or the bone of control animals. Osteoclast activity in the implanted area was also higher than the other portions of the bone or the bone of control animals. Replacement of the intraosseous residual β-TCP granules for bone progressed at 12 weeks after implantation compared to those at 8 weeks after implantation. These data suggested that the spherical β-TCP granules stimulated osteogenesis and osteoclast activity of the unloaded bone.

Introduction

Beta-tricalcium phosphate (β-TCP) has been used clinically as a bioresorbable bone substitute. In addition to the porosity and the structure of micro and macro pores, microstructure of the particles composing the material has also been shown to be associated with the bioresorbability [1]. We have shown that the cylindrical block of β-TCP composed of unique rod-shaped particles behaved differently from the same-shaped block of conventional β-TCP composed of non rod-shaped particles when implanted into rabbit femurs, and proposed the hypothesis that bioresorbability of the bone substitute affected the metabolism of the subsequently formed bone tissue [2]. Previously, we also have developed spherical granules of β-TCP using a new unique method [3]. After implantation into rat femurs, both spherical β-TCP granules composed of rod-shaped particles produced by hydrothermal method and β-TCP granules composed of non rod-shaped particles revealed good osteoconductivity. Total volume of the newly formed bone and implant was similar

between animals implanted β-TCP composed of rod-shaped particles and animals implanted β-TCP composed of non rod-shaped particles, but the volume of newly formed bone/total volume of newly formed bone and implant was higher in the animals implanted β-TCP granules composed of rod-shaped particles than the animals implanted β-TCP granules composed of non rod-shaped particles [4]. In this study, we analyzed osteoconductivity and bioresorbability of spherical β-TCP granules composed of rod-shaped particles in the bone with reduction in osteogenic potential induced by mechanical unloading [5].

Materials and Methods

Production of Spherical β-TCP Granules: Alpha-TCP powder was mixed and kneaded with gelatine, and dropped into stirring oil bath heated at 80°C. Then, the bath was chilled on ice and formed spherical α-TCP granules. The granules were separated from the oil, rinsed, and served for hydrothermal treatment to produce spherical β-TCP granules composed of rod-shaped particles [6]. The size was ranged from 0.5 to 0.6 mm in diameter. The synthesized spherical β-TCP granules were analyzed by X-ray diffractometry, and no phase other than β-TCP was detected. Rod-shaped particles of spherical β-TCP granules were confirmed using a scanning electron microscope.

Animal Experiments: Eight-week-old female Wistar rats were anesthetized, a bone defect 2 mm in diameter and 3 mm in depth was created in distal end of the right femur of each animal, 30 mg of β-TCP granules were implanted and the wound portion was sutured. Operated animals without implantation of β-TCP granules were used as a control. The right sciatic neurectomy was performed 2 weeks before euthanization. Four, 8 and 12 weeks after implantation, animals were euthanized and operated bones were resected. Undecalcified bone tissue sections were made from the resected bones and analyzed histologically. Rearing of these animals and animal experiments were performed following the Guidelines of Animal Experimentation of Nagasaki University.

Results and Discussion

Right tibiae 2 weeks after sciatic neurectomy revealed growth retardation and decreased bone mass compared to the left tibiae without neurectomy, and unloading of the right limb was confirmed. In the operated right femur, regeneration of the non-critical sized bone defect in the unloaded bone was apparently delayed compared to the loaded bone (data not shown). Four weeks after implantation, newly formed bone appeared around the partially resorbed implant. Bone regeneration occurred from marginal region of the bone defect and implanted β-TCP granules in the marginal region of operated area were already surrounded by newly formed bone. In central region of the operated area, connective tissue still remained (Fig. 1A). Marginal region of the bone defect of control animals was partly regenerated, but most part of the defect remained and was filled with connective tissue (Fig. 1B). At 8 weeks after implantation, prominent bone formation was seen in and around the implant in contrast to the control (Fig. 1C, D). Greater numbers of tartrate-resistant acid phosphatase-positive cells were present around the implant than those in the other portions of the bone and in the control bone (data not shown). At 12 weeks after implantation, histological findings were similar to those at 8 weeks after implantation (Fig. 1E). Total volume of the implant and newly formed bone was much more than the other portions of the bone in the animals 8 weeks and 12 weeks after implantation. In the control bone, the created bone defect was mostly regenerated at 8 weeks after operation, the bone defect were mostly regenerated. At 12 weeks after operation the cancellous bone which was formed in the created bone defect was indistinguishable from surrounding slender cancellous bone under mechanical unloading (Fig. 1D, F). Under polarizing microscope, refringence of lamellar structure of bone enables to distinguish implanted β-TCP granules from bone tissue. As shown in Fig. 2A, considerable amount of β-TCP embedded in the bone was seen in the specimens 8 weeks after implantation. At 12 weeks after implantation, part of the embedded β-TCP granules was replaced by bone and newly formed bone was seen within the implanted granules (Fig. 2B). Total volume

of newly formed bone in the animals implanted with β-TCP granules was significantly higher than that in control animals created the bone defect. These data suggested that the spherical β-TCP granules stimulated osteogenesis and osteoclast activity in the unloaded bone. In addition, it was also suggested that replacement of the intraosseous residual β-TCP granules for bone occurred in the suppressive osteogenetic conditionunder the mechanical unloading.

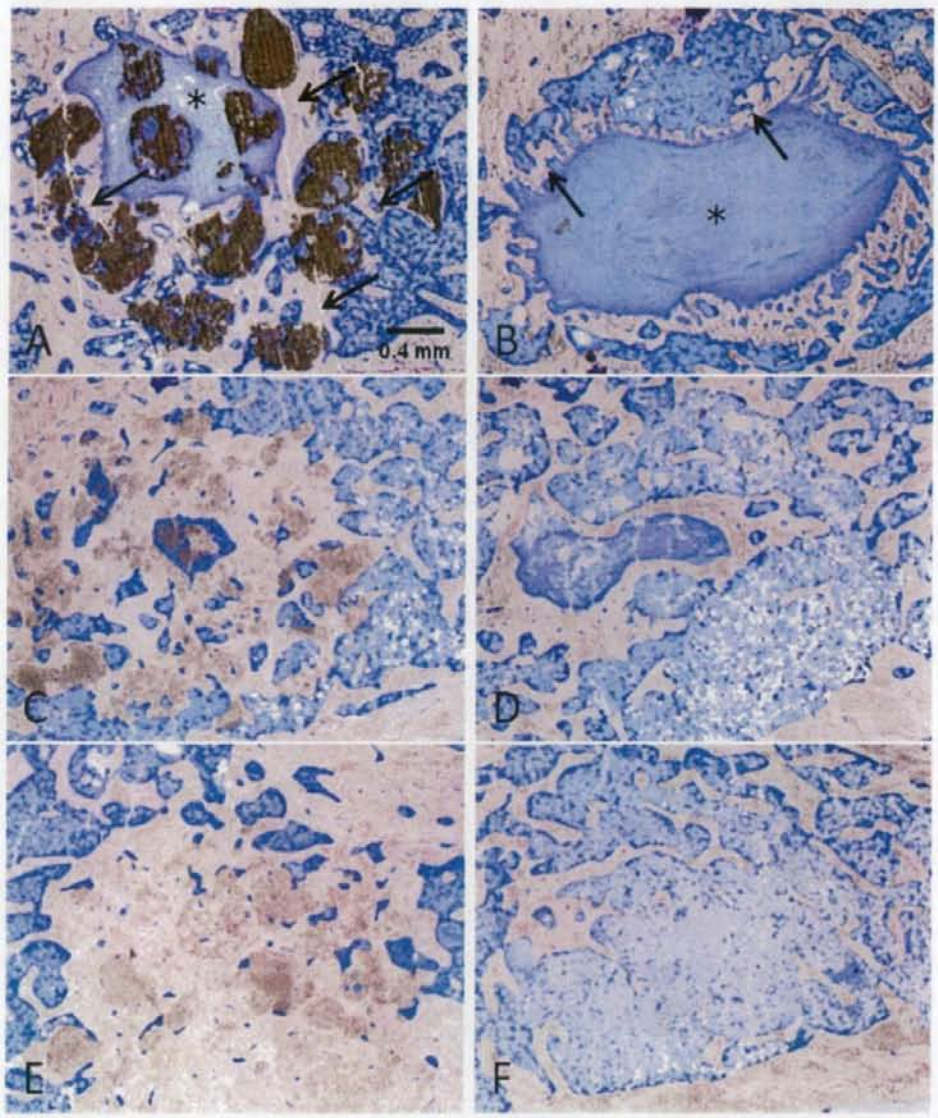

Fig. 1 Representative photomicrograph of specimens implanted with spherical β-TCP granules (A, C, E) and control specimens without implantation into the bone defects (B, D, F). Specimens 4 weeks (A, B), 8 weeks (C, D) and 12 weeks after operation (E, F) were stained with Giemsa's method. For all specimens, sciatic neurectomy was performed 2 weeks before sampling for histological analyses. Arrows indicate newly formed bone in marginal region. Asterisks (*) represent connective tissue in the bone defect.

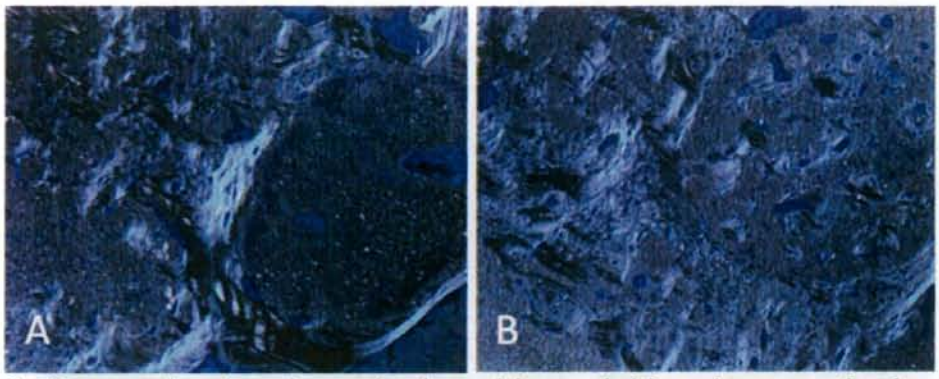

Fig. 2 Representative photomicrographs observed by a polarizing microscope. Specimens 8 weeks (A) and 12 weeks (B) after implantation of spherical β-TCP granules.

References

[1] H. Yokozeki, T. Hayashi, N. Nakagawa, H. Kurosawa, K. Shibuya and K. Ioku. *J. Mater. Sci. Mater. Med.* **9**:381-384. (1998)

[2] T. Okuda, K. Ioku, I. Yonezawa, H. Minagi, G. Kawachi, Y. Gonda, H. Murayama, Y. Shibata, S. Minami, S. Kamihira, H. Kurosawa and T. Ikeda. *Biomaterilas* **28**:2612-2621. (2007)

[3] K. Ioku, G. Kawachi, S. Sasaki, H. Fujimori, S. Goto. *J. Mater. Sci.* **41**:1341-1344. (2006)

[4] Y. Gonda, K. Ioku, T. Okuda, G. Kawachi, I. Yonezawa, H. Kurosawa, T. Ikeda. *Key Eng. Mater.* **361-363**:1013-1016. (2008)

[5] M. Weinreb, G. A. Rodan, D. D. Thompson. *Bone* **10**:187-194. (1989)

[6] K. Ioku, M. Kamitakahara, G. Kawachi, Y. Gonda, T. Okuda, I. Yonezawa, H. Kurosawa, T. Ikeda, *Key Eng. Mater.* **361-363**:989-992. (2008)

Available online at www.sciencedirect.com
ScienceDirect
Mutation Research 638 (2008) 48–55
Fundamental and Molecular Mechanisms of Mutagenesis
www.elsevier.com/locate/molmut
Community address: www.elsevier.com/locate/mutres

Mutagenic radioadaptation in a human lymphoblastoid cell line

Fumio Yatagai [a,*], Yukihiro Umebayashi [a], Masamitsu Honma [b], Kaoru Sugasawa [c], Yuko Takayama [a], Fumio Hanaoka [d]

[a] *Advanced Development and Support Center, The Institute of Physical and Chemical Research (RIKEN), Saitama 351-0198, Japan*
[b] *Division of Genetics and Mutagenesis, National Institute of Health Sciences, Tokyo 158-8501, Japan*
[c] *Genome Damage Response Research Unit, The Institute of Physical and Chemical Research (RIKEN), Saitama 351-0198, Japan*
[d] *Graduate Program, Frontiers in Biosciences, Osaka University, Osaka 565-0871, Japan*

Received 6 April 2007; received in revised form 15 August 2007; accepted 22 August 2007
Available online 1 September 2007

Abstract

We investigated the mutagenic radioadaptive response of human lymphoblastoid TK6 cells by pretreating them with a low dose (5 cGy) of X-rays followed by a high (2 Gy) dose 6 h later. Pretreatment reduced the 2-Gy-induced mutation frequency (MF) of the *thymidine kinase* (*TK*) gene (18.3×10^{-6}) to 62% of the original level (11.4×10^{-6}). A loss of heterozygosity (LOH) detection analysis applied to the isolated TK^{-} mutants revealed the mutational events as non-LOH (resulting mostly from a point mutation in the *TK* gene), hemizygous LOH (resulting from a chromosomal deletion), or homozygous LOH (resulting from homologous recombination (HR) between chromosomes). For non-LOH events, pretreatment decreased the frequency to 27% of the original level (from 7.1×10^{-6} to 1.9×10^{-6}). cDNAs prepared from the non-LOH mutants revealed that the decrease was due mainly to the repression of base substitutions. The frequency of hemizygous LOH events, however, was not significantly altered by pretreatment. Mapping analysis of chromosome 17 demonstrated that the distribution and the extent of hemizygous LOH events were also not significantly influenced by pretreatment. For homozygous LOH events, pretreatment reduced the frequency to 61% of the original level (from 5.1×10^{-6} to 3.1×10^{-6}), reflecting an enhancement in HR repair of DNA double-strand breaks. Our findings suggest that the radioadaptive response in TK6 cells follows mainly from mutations at the base-sequence level, not the chromosome level.

Keywords: Adaptive response; TK6 cells; LOH detection system

1. Introduction

An adaptive cellular response occurs when a mild stress applied before a challenging treatment with a DNA-damaging agent decreases the detrimental effects of the challenge. In radioadaptation, as it is usually defined, exposure to a low dose of ionizing radiation (IR) provides some protection against a high dose. Radioadaptation was first reported by Olivieri et al. [1], who showed that radiation delivered by labeling human lymphocytes with tritiated thymidine causes a decrease in the frequency of chromosomal aberrations induced by subsequent exposure to 15 Gy of IR. That discovery stimulated a series of studies in human lymphocytes and various mammalian cell lines (for review, see refs. [2,3]) and suggested that the adaptive response is an important defense mechanism, especially against low doses of IR. The molecular mechanisms involved, however, remain largely unknown [4–8], and cellular

* Corresponding author. Tel.: +81 48 467 9710; fax: +81 48 462 1426.
E-mail address: yatagai@postman.riken.go.jp (F. Yatagai).

0027-5107/$ – see front matter © 2007 Elsevier B.V. All rights reserved.
doi:10.1016/j.mrfmmm.2007.08.014

responses such as the bystander effect, genetic instability and hyper-radiosensitivity seem tightly related to the adaptive response in a specific low-dose region. One of the hot subjects in recent adaptive response studies is the expression of the genes involved in the mechanism [8–10]. Another is the relationship between the adaptive response and the bystander effect [11–15]. In mammalian cells, for example, bystander mutagenesis may be suppressed by an adaptive response [11].

Following the report by Olivieri et al., reduced induction of both micronuclei and sister chromatid exchanges was shown in Chinese hamster V79 cells pre-exposed to low doses of γ-rays or ^{3}H β-rays [16]. Subsequent studies reported similar radioadaptive responses, such as reduced mutation frequencies in human lymphocytes [17], mouse SR-1 cells [18] and human–hamster hybrid A_L cells [19], an altered mutation spectrum in human–hamster hybrid A_L cells [19], reduced micronucleus frequencies in human lymphocytes [5] and mouse embryo cells [20], and reduced deletions and rearrangements in human lymphoblast cells [21]. The mechanism underlying those radioadaptations may have been the induction of an efficient chromosome repair system by the priming radiation dose, and in fact, the efficiency of DNA double-strand break (DSB) repair in Chinese hamster V79 cells exposed to γ-rays is enhanced by a priming exposure of 5 cGy of γ-rays [22]. Furthermore, DSBs with either blunt or staggered ends, created by restriction enzymes, induce the adaptive response [3].

The human lymphoblastoid TK6 cell line, isolated by Skopek et al. [23], is heterozygous at the *thymidine kinase* (*TK*) locus. Honma's laboratory developed a loss of heterozygosity (LOH) detection system that can be used for molecular analysis of *TK* mutations as well as for detecting alterations at the chromosome level [24,25]. Using that methodology, we were able to detect IR effects at doses as low as 10 cGy [26–28]. Irradiation of TK6 cells with 10 cGy of X-rays clearly demonstrated radiation-specific types of LOH events or interstitial deletions in chromosome 17 [26]. We also observed more efficient induction of such events after 10 cGy irradiation with an accelerated carbon-ion (135 MeV/u) beam [27], and this was apparent in frozen cells exposed to the same carbon-ion beam [28]. These results strongly suggest that the interstitial deletions were the result of end-joining repair of IR-induced DSBs.

Because the radiation-sensitive LOH analysis system in TK6 cells is effective for detecting the fate of radiation-induced DNA double-strand breaks (DSBs), we use it here to see if the adaptive response could produce measurable changes in IR-induced genetic alterations. The results we obtained were not completely expected, but are interesting.

2. Materials and methods

2.1. Cell culture and adaptive treatment

The methodologies for the detection of *TK*-deficient mutants and the materials and methods used for cell culture and growth have been previously reported [26]. Briefly, TK6 cells were incubated in RPMI1640 medium supplemented with HAT to eliminate pre-existing TK^- deficient mutants. The cells were then resuspended in fresh normal medium, and 6 ml cell suspension was dispensed into 6-cm diameter Petri dishes. The cells were pretreated ("primed") with 2.5, 5 or 10 cGy of X-rays (250 kVp) at a rate of 10 cGy/min, and placed in a 5% CO_2 humidified incubator. The cell concentration was adjusted to 8×10^5 cells/ml at the end of the post-irradiation incubation period of 1.5, 3, 6, 9 or 12 h. The cells were then challenged with 2 Gy X-rays (250 kVp) at 1 Gy/min. Non-primed irradiated cells treated in the same manner as the primed cells served as controls.

2.2. Survival assay and TK mutation assay

To determine the surviving fraction of the challenged cells, we measured the plating efficiency (PE) immediately after irradiation using the limiting dilution method. For mutation expression, we incubated the cells with non-selecting RPMI1640 medium for about 60 h following the X-ray challenge. We measured the PE of incubated cells similarly, determining the *TK* mutation frequency. To select TK^- mutant clones, we seeded incubated cells into 96-well plates at 4×10^4 cells per well in RPMI1640 medium containing 4 μg/ml trifluorothymidine (TFT); we harvested the normally growing clones after 2 weeks and the slow growing clones after 4 weeks.

2.3. Determination of optimum irradiation conditions for mutagenic adaptation

To determine the optimum conditions for evoking the mutagenic radioadaptive-response, we tested the MF induced by 2 Gy at 0, 1.5, 3, 6, 9 and 12 h after a priming dose of 10 cGy, selected the optimum interval time, and then tested the MF induced by 2 Gy at that interval time after priming doses of 0, 2.5, 5 and 10 cGy.

2.4. LOH analysis of TK^- mutants

Fig. 1 illustrates how we classified TK^- mutants. We first determined *TK* LOH by PCR analysis of exons 4 and 7 [29]. If the PCR products of both were similar to those of the parental *TK* heterozygous cells, we classified the mutant

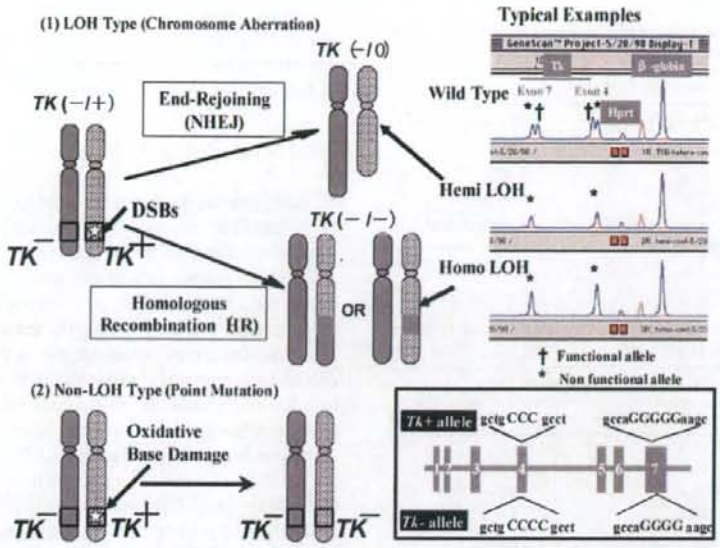

Fig. 1. LOH classifications of TK^- mutants. The first step in the genetic analysis of selected TK^- mutants was to judge whether there was a loss of *TK* heterozygosity (LOH). This was accomplished by PCR amplification of exons 4 and 7 regions of the *TK* locus. This step also distinguished between hemizygous LOH (loss of the functional *TK* allele) and homozygous LOH (replacement of the functional *TK* allele by a mutated TK^- allele (see ref. [29]).

as a "non-LOH" mutant. We used the same technique to distinguish between hemizygous LOH (in which the functional *TK* allele is lost) and homozygous LOH (in which the functional *TK* allele is replaced by TK^-). To determine the extent and size of the deleted or substituted portions of the chromosome involved, we analyzed 11 microsatellite regions (D17S588, D17S1784, D17S785, D17S789, D17S802, D17S807, D17S928, D17S932, D17S1299, D17S1566 and THRA) on chromosome 17 using multiple PCR reactions as described previously [29]. The fine structure of the recovered TK^- LOH mutations was determined by chromosome mapping analysis.

2.5. Base sequencing of non-LOH mutants

For a precise analysis of non-LOH mutants, we extracted RNA using Isogen (Nippon Gene, Japan), and obtained cDNA using a First-Strand cDNA Synthesis Kit, Amersham, USA). Following PCR amplification, the purified 807-bp fragments were sequenced by Takara Bio (Japan). The primers 5′-AGAGTACTCGGGTTCGTGAA-3′ and 5′-GCAGCATGCAGGGCAGCGTG-3′ (forward and reverse, respectively) were used for cDNA synthesis, PCR amplification and base sequencing [30]. To prevent the overestimation of mutational events, we counted identical mutations originating from a single irradiated dish as a single event.

Table 1a
TK mutation frequency (MF) at various time intervals between priming and challenging X-ray exposures (priming dose, 10 cGy; challenging dose, 2 Gy)

Time interval (h)	0	1.5	3	6	9	12
TK MF ($\times 10^{-6}$)	19.8	18.1	14.4	13.5	17.8	19.7

3. Results

3.1. Optimum conditions for mutagenic adaptation

For inducing an adaptive response to X-ray irradiation, the optimum interval between a 10-cGy priming dose and a 2-Gy challenging dose was 6 h (Table 1a), and the optimum priming dose 6 h prior to a 2-Gy challenging dose was 5 cGy (Table 1b). We therefore decided to characterize the induced *TK* mutants by repeating

Table 1b
TK mutation frequency at various priming X-ray doses (challenging dose, 2 Gy; interval between 2 exposures, 6 h)

Priming X-ray dose (cGy)	0	2.5	5	10
TK MF ($\times 10^{-6}$)	13.3	15.8	4.5	6.3

Table 2
Surviving fractions of primed and non-primed TK6 cells following challenge exposure to 2 Gy X-rays

Experiment	Surviving fraction	
	Non-primed cells	Primed cells (5 cGy)
I	0.043	0.047
II	0.047	0.070
III	0.049	0.040
Mean ± S.D.	0.046 ± 0.0031*	0.052 ± 0.016*

* $P = 0.58$; t-test.

Table 3
TK mutation frequency in primed and non-primed TK6 cells following challenge exposure to 2 Gy X-rays

Experiment	*TK* mutation frequencies ($\times 10^{-6}$)	
	Non-primed cells	Primed cells (5 cGy)
I	13.3	4.5
II	13.3	10.5
III-a	20.4	15.1
III-b	21.0	15.6
Mean ± S.D.	18.3 ± 4.3*	11.4 ± 5.1*

Experiments III-a and III-b were carried out concurrently with survival assay III, but they were independent mutation assays.
* $P = 0.020$; t-test.

our mutation experiments under those conditions (5 cGy followed 6 h later with 2 Gy).

3.2. Survival assay and TK mutation assay

Table 2 shows the surviving fraction, expressed as PE (2 Gy X-ray irradiated cells)/PE (unirradiated cells) of primed and unprimed cells immediately after the 2-Gy challenge exposure. Irradiation with the priming dose of 5 cGy did not influence the PE of unchallenged cells (data not shown). The effect of priming on survival after 2 Gy X-ray irradiation was 1.1 (0.052/0.046; $P = 0.58$, t-test). Thus, priming did not significantly affect survival after the challenge exposure.

On the other hand, priming did affect the *TK* MF induced by the challenge. Data from 4 independent experiments showed that priming reduced the MF to 62% of the unprimed MF ($P = 0.020$, t-test) (Table 3).

3.3. LOH analysis of TK^- mutants

Table 4 shows the distributions of LOH classes among the isolated TK^- mutants as determined by PCR analysis. We isolated non- and "small" LOH mutants (see Sections 3.4 & 3.5) as normal growth mutants in the first selection, except for a few cases. We isolated the remaining LOH mutants as slow growth mutants in the second selection. We estimated the pre-exposure effect from the proportion of each mutational event as follows: (i) 7.1×10^{-6} to 1.9×10^{-6} reduction in corresponding MF of non-LOH events, (ii) 6.4×10^{-6} to 6.1×10^{-6} change in corresponding MF of hemizygous LOH events and (iii) 5.1×10^{-6} to 3.1×10^{-6} reduction in corresponding MF of homozygous LOH events. Thus, the MF of a non-LOH event in primed cells was reduced to 27% of the non-primed MF. The induction of hemizygous events, on the other hand, was barely influenced by priming. As far as homozygous events go, their corresponding MF was reduced to 61% of the original level, which was similar to level of reduction in total MF (62%).

3.4. Analysis of LOH tracts on chromosome 17

Fig. 2 shows the deleted or replaced regions of chromosome 17 in each LOH mutant. Mutants reflected both type 1 and type 2 LOH events. Type 1 defines a terminal event; that is, the deleted or exchanged chromosome segment extends to the telomere marker (D17S928). Type 2 defines an interstitial deletion; the altered segment does not reach the telomere marker.

In the present study, most hemizygous LOH mutations, which are considered to be the result of DSB non-homologous end-joining (NHEJ) repair, reflected

Table 4
Distribution of mutational classes among the isolated *TK* mutants

Mutational class	Number of identified mutants (Exp. I, II, III-a, III-b) [MF $\times 10^{-6}$]	
	Non-primed cells	Primed cells (5 cGy)
Non-LOH	18 (5, 4, 6, 3) [7.1]	8 (1, 3, 2, 2) [1.9]
LOH		
Hemizygous	15 (3, 3, 7, 2) [6.0]	27 (8, 7[a], 5, 7) [6.4]
Homozygous	13 (3, 4, 3, 3) [5.1]	13 (2, 3, 5, 3) [3.1]
Total	46 (11, 11, 16, 8) [18.3]	48 (11, 13, 12, 12) [11.4]

[a] One of the seven mutants was a mixed hemizygous/homozygous type.

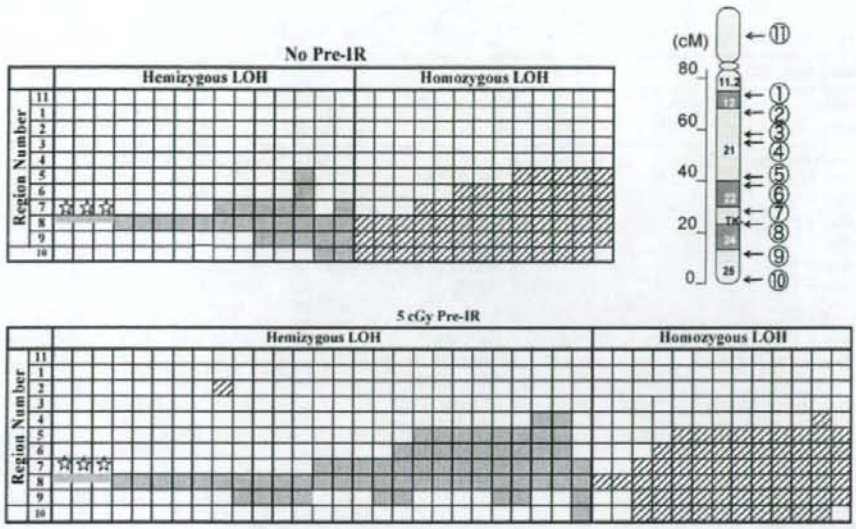

Fig. 2. Chromosome mapping of the LOH mutants. We analyzed the LOH mutants selected after a 2 Gy of challenging X-ray irradiation to determine the extent of the deleted or exchanged portions of the chromosome. The upper panel shows the profiles of 28 LOH mutants selected from non-primed cells, and the lower panel shows the profiles of 40 LOH mutants selected from cells primed with 5 cGy of X-rays. Each column represents a single LOH mutant. The rows represent regions of chromosome 17 diagrammed in the upper right insert. Shaded squares represent deleted regions and hatched squares represent exchanged regions (see text). The region numbers refer to the 11 microsatellite regions: (1) D17S588; (2) D17S1784; (3) D17S785; (4) D17S789; (5) D17S802; (6) D17S807; (7) D17S928; (8) D17S932; (9) D17S1299; (10) D17S1566; (11) THRA (see ref. [29]). The star symbol represents a "small" type 2 hemizygous event in which the deletion is restricted to *TK* locus.

type 2 events in both the non-primed (13 of 15 mutants) and primed (26 of 27 mutants) groups. Small type 2 deletions – those restricted to the *TK* locus (Fig. 2) – were infrequent in both groups (3 of 15 mutants in non-primed cells and 3 of 27 in primed cells). Similarly, the proportion of large deletion mutants (expanding to the region beyond region 8, Fig. 2) was also similar in the primed (18 of 27 mutants) and non-primed (7 of 15 mutants) groups. Homozygous LOH events, on the other hand, which are considered to be the result of homologous recombination (HR) repair of DSBs, were primarily identified as type 1 events in both primed (10 of 13) and non-primed (12 of 13) groups. Interestingly, small homozygous LOH events (where only a single region was replaced, Fig. 2) were recovered from the primed cells (2 of 13 (3 0f 14)), but not from the non-primed cells (0 of 13).

3.5. Analysis of non-LOH-mutants

We detected many types of alterations in the non-LOH mutant cDNAs (Table 5). The proportion of single base-substitutions among all the mutations identified as this class was 1/8 (13%) in the primed cells, and this value was clearly lower than 7/18 (87%) in the unprimed cells. G and C bases were targeted in base substitution mutations, except for a single case of an A to T transversion (Table 5). Most (4/5) of the double-base changes consisted of a single base deletion (causing a frameshift) and a base substitution, except for a single case of a GC to TA double transversion in a radioadapted mutant. It is difficult to estimate the effect of priming on the induction of the double-base change events from the limited number of cells involved. Similar difficulties were also found in the other mutational events in this class such as triple-base changes, multiple-base changes and exon skipping. In addition, the proportion of abnormal transcription events (both functional and non-functional *TK* alleles are equally transcribed) was also similar in the radioadapted (1/8, 13%) and the non-adapted (3/18, 17%) group, although its origin was not identified.

4. Discussion

The radioadaptation conditions used in this study (5 cGy of priming X-rays followed in 6 h by 2 Gy of challenging X-rays) were similar to those used in other studies [4,6,11,12,14,16]. The *TK* mutation frequency

Table 5
Nature of the isolated non-LOH mutants

Type of mutation		Number of identified mutants	
Specific changes	[Position: exon]	Non-primed exposure	Primed (5 cGy) pre-X-ray
Single base substitutions		7	1
G → A (Gly → Glu)	[56:1]	3	0
C → T (Gln → Stop)	[64:1]	1	0
C → A (Ser → Stop)	[89:2]	1	0
A → T (Ser → Cys)	[97:2]	1	0
G → C (Leu → Phe)	[108:2]	0	1
G → A (Glu → Lys)	[430:6]	1	0
Double base changes		3	2
G → A (Gly → Glu)/Del. C	[56:1/676:7]	1	0
G → C (Leu → Phe)/Del. A	[108:2/686:7]	0	1
Add. C/Del. G	[232:4/641:7]	1	0
GC → TA (Leu Asp → Leu Asn)	[372 and 373:5]	0	1
G → A (Glu → Lys)/Del. G	[430:6/447:6]	1	0
Triple base changes		0	1
Del. G/C → T (Ile → Ile)/C → T (Leu → Leu)	[92:1/288:4/561:7]	0	1
Multiple base changes		1	1
CC → AT (Thr Gln → Thr Stop)/G → A (Gln → Gln)/G → A (Gln → Gln)/Add. C/Del. G	[51 and 52:1/66:1/667:7/232:4/641:7]	0	1
Base changes at 20 sites		1	0
Exon skipping, abnormal splicing and deletion		3	2
Del. of a part of exon 1 (48 bases)	[161–209: 1]	1	1
Abnormal splicing of intron (between exons 1 and 2)		1	0
Skipping of exon 3 (Del. 111 bases)	[99–203: 3]	1	0
Skipping of exon 5 (Del. 90 bases)	[304–393: 5]	0	1
Abnormal transcription		3	1
Both functional and non-functional alleles are equally transcribed			
Unidentified		1	0
Total		18	8

we observed after the challenge X-rays (18.3×10^{-6}) was reduced by the 5-cGy priming exposure to about 62% of the non-primed level (11.4×10^{-6}). Taking into consideration the *TK* spontaneous mutation frequency observed in our recent study (3.0×10^{-6}) [32], the increase in MF induced by 2 Gy of X-rays was reduced from 6.1-fold to 3.8-fold.

We originally planned this study to determine whether radioadaptation would alter the characteristics of X-ray-induced LOH events. X-ray-induced interstitial deletions are likely to be the result of NHEJ repair of DSBs, and this type of mutation was the one we recovered most frequently after 2 Gy X-ray irradiation in our previous study [24]. We also found that carbon-ion beam irradiation induced interstitial deletions more efficiently than the same dose of X-rays [26,27], which we interpreted as the result of a higher occurrence of inaccurately repaired DSBs. In the present study, however, we found that the frequency of hemizygous LOH mutations, as well as their size and the distribution of deleted regions on chromosome 17, was similar for radioadapted and non-adapted cells. Those results are not consistent with reports suggesting that enhanced repair of DSBs reduces chromosomal alterations [21,22]. An entire genome assay might lead to results similar to the ones in those reports, but our observations were restricted to the *TK* locus on chromosome 17.

On the other hand, we observed a decrease in the induction of homozygous LOH events in the primed cells, which suggests that priming enhanced the HR repair of DSBs. We recently constructed a model system to follow the fate of a single DSB introduced by the restriction enzyme I-sceI at a specific site in the *TK* gene in TK6 cells [31]. In preliminary exper-

iments, low dose/low-dose rate γ-irradiation (30 mGy at 1.2 mGy/h) did not significantly affect end joining (EJ) repair of this specific DSB, but it enhanced the efficiency of HR repair by about 50% (unpublished data). The small homozygous LOH events we observed in the primed cells in the present study (3/14) might reflect this enhanced HR, but we must examine whether the adaptive response was really involved because we also recovered small homozygous LOH mutants after the low-dose/low-dose rate γ-ray exposures [32]. The decrease in the frequency of single-base substitutions that we observed in primed cells (1/48) versus non-primed cells (7/46) (Tables 4 and 5) is rarely influenced by counting base substitutions accompanied by single base deletions (which would result in 2/48 for primed cells and 9/46 for non-primed cells), so the most likely mechanism for the reduced induction of non-LOH mutants was suppression of base substitutions.

One of the possible targets for radioadaptation is oxidative base damage. In fact, down-regulation of the human *CDC16* gene that occurs after oxidative stress causes more rapid and efficient repair in adapted (2 cGy pre-irradiated) human lymphoblastoid cells challenged with 4 Gy irradiation [6]. On the other hand, oxidative base excision repair enzymes, including DNA glycosylases, hOGG1 and hNth1, are reportedly not up-regulated at the post-transcriptional level in γ-ray-primed TK6 cells [33]. Since DNA glycosylase can suppress base substitution, we need to examine whether radioadaptation enhances the enzyme's activity under the present condition. Alternatively, base substitution activity might not accurately reflect DNA glycosylase activity because attempted base excision repair of IR damage by the enzyme can lead to lethal and mutagenic DSBs [34].

A variety of untargeted effects may contribute to the short- and long-term fate of a cell exposed to IR [35]. An example is the possible involvement of a "radioadaptive bystander" effect in human lung fibroblasts [36]. The reduction of radiosensitivity in cells with a wild type *p53* gene by a radiation-induced, nitric oxide (NO)-mediated bystander effects may be a manifestation of the radioadaptive response [37,38]. This possibility is supported by the finding that the NO-induced apoptosis observed in lymphoblastoid and fibroblast cells depends on the phosphorylation and activation of p53 [39]. However, it is still unclear whether the NO-mediated pathway also contributes to the mutagenic adaptation. The de novo protein synthesis is required for expression of adaptive responses [22,40], and gene expression studies are improving our understanding of the molecular mechanisms underlying the radioadaptive response [9,10,40,41]. Our laboratory is also focusing on the molecular mechanisms involved in radioadaptation, especially the expression of genes involved in DNA base and nucleotide excision repair.

Acknowledgements

This study was partially supported by the Budget for Nuclear Research of the Ministry of Education, Culture, Sports, Science and Technology, and was reviewed by the Atomic Energy Commission of Japan. We thank Dr. Miriam Bloom (SciWrite Biomedical Writing & Editing Services) for professional editing.

References

[1] G. Olivieri, Y. Bodycote, S. Wolf, Adaptive response of human lymphocytes to low concentrations of radioactive thymidine, Science 223 (1984) 594–597.
[2] S. Wolf, Aspects of the adaptive response to very low doses of radiation and other agents, Mutat. Res. 358 (1996) 135–142.
[3] S. Wolf, The adaptive response in radiobiology: evolving insights and implications, Environ. Health Pesrpect. 106 (1998) 277–283.
[4] O. Rigaud, E. Moustacchi, Radioadaptation for gene mutation and the possible molecular mechanisms of the adaptive response, Mutat. Res. 358 (1996) 127–134.
[5] M. Wojewodska, M. Kruzewski, K. Iwanenko, I. Szumiel, Effects of signal transduction in adapted lymphocytes: micronuclei frequency and DNA repair, Int. J. Radiat. Biol. 71 (1997) 245–252.
[6] P.-K. Zhou, O. Rigaud, Down-regulation of the human *CDC16* gene after exposure to ionizing radiation: a possible role in the radioadaptive response, Radiat. Res. 155 (2001) 43–49.
[7] M.S. Sasaki, Y. Ejima, A. Tachibana, T. Yamada, K. Ishizaki, T. Shimizu, T. Nomura, DNA damage response pathway in radioadaptive response, Mutat. Res. 504 (2002) 101–118.
[8] I. Szumiel, Adaptive responses: stimulated DNA repair or decreased damage fixation? Int. J. Radiat. Biol. 81 (2005) 233–241.
[9] M.A. Coleman, E. Yin, L.E. Peterson, D. Nelson, K. Sorensen, J.D. Tucker, A.J. Wyrobeck, Low-dose irradiation alters the transcript profiles of human lymphoblastoid cells inducing genes associated with radioadaptive response, Radiat. Res. 164 (2005) 369–382.
[10] H.P. Wang, X.H. Long, Z.Z. Sun, O. Rigaud, Q.Z. Xu, Y.C. Huang, J.L. Sui, B. Bai, P.K. Zhou, Identification of differentially transcribed genes in human lymphoblastoid cells irradiated with 0.5 Gy of γ-ray and the involvement of low dose radiation inducible CHD6 gene in cell proliferation and radiosensitivity, Int. J. Radiat. Biol. 82 (2006) 181–190.
[11] S.G. Swant, G. Randers-Pehrson, N.F. Metting, E.J. Hall, Adaptive response and the bystander effect induced by radiation in C3H 10T1/2 cells in culture, Radiat. Res. 156 (2001) 177–180.
[12] H.N. Zhou, G. Randers-Pehrson, C.R. Geard, D.J. Brenner, E.J. Hall, T.K. Hei, Interaction between radiation-induced adaptive response and bystander mutagenesis in mammalian cells, Radiat. Res. 160 (2003) 512–516.
[13] W.M. Bonner, Thresholds, bystander effect, and adaptive response, Proc. Natl. Acad. Sci. U.S.A. 100 (2003) 4973–4975.
[14] S.A. Mitchell, S.A. Marino, D.J. Brenner, E.J. Hall, Bystander effect and adaptive response in C3H 10T(1/2) cells, Int. J. Radiat. Biol. 80 (2004) 465–472.

[15] T.K. Hei, R. Persaud, H. Zhou, M. Suzuki, Genotoxicity in the eyes of bystander cells, Mutat. Res. 568 (2004) 111–120.
[16] T. Ikushima, Chromosomal response to ionizing radiation reminiscent of an adaptive response in cultured Chinese hamster cells, Mutat. Res. 180 (1987) 215–221.
[17] B.J.S. Sanderson, A.A. Morely, Exposure of human lymphocytes to ionizing radiation reduces mutagenicity by subsequent radiation, Mutat. Res. 164 (1986) 151–347.
[18] P.K. Zhou, X.Y. Liu, W.Z. Sun, Y.P. Zhang, Y.P.K. Wei, Cultured mouse SR-1 cells exposed to low-dose of γ-rays become less susceptible to the induction of mutations by radiation as well as bleomycin, Mutagenesis 8 (1993) 109–111.
[19] A.M. Ueno, D.B. Vannais, S.L. Gustafson, J.C. Wong, C.A. Waldren, A low adaptive dose of gamma-rays reduced the number and altered the spectrum of S1 mutants in human hamster hybrid cells, Mutat. Res. 358 (1996) 161–169.
[20] E.I. Azzam, G.P. Raaphorst, R.E. Mitchel, Radiation-induced adaptive response for protection against micronucleus formation and neoplastic transformation in C3H 10T1/2 mouse embryo cells, Radiat. Res. 138 (1994) S28–S31.
[21] O. Rigaud, D. Papadopoulo, E. Moustacchi, Decreased deletion mutation in radioadapted human lymphoblast, Radiat. Res. 133 (1993) 94–101.
[22] T. Ikushima, H. Aritomi, J. Morisita, Radioadaptive response: efficient repair of radiation-induced DNA damage in adapted cells, Mutat. Res. 358 (1996) 193–198.
[23] T.R. Skopek, H.L. Liber, B.W. Penman, W.G. Thilly, Isolation of a human lymphoblastoid line heterozygous at the thymidine kinase locus: possibility for a rapid human cell mutation assay, Biochem. Biophys. Res. Commun. 84 (1978) 411–416.
[24] M. Honma, M. Hayashi, T. Sofuni, Cytotoxic and mutagenic responses to X-rays and chemical mutagens in normal and p53-mutated human lymphoblastoid cell, Mutat. Res. 374 (1996) 89–98.
[25] M. Honma, L.S. Zhang, M. Hayashi, K. Takeshita, Y. Nakagawa, N. Tanaka, T. Sofuni, Illegitimate recombination leading to allelic loss and unbalanced translocation in p53-mutated human lymphoblastoid cells, Mol. Cell. Biol. 17 (1997) 4774–4781.
[26] S. Morimoto, T. Kato, M. Honma, M. Hayashi, F. Hanaoka, F. Yatagai, Detection of genetic alterations induced by low-dose X rays: analysis of loss of heterozygosity for *TK* mutation in human lymphoblastoid cells, Radiat. Res. 157 (2002) 533–538.
[27] S. Morimoto, M. Honma, F. Yatagai, Sensitive detection of LOH events in a human cell line after C-ion beam exposure, J. Radiat. Res. 43 (Suppl.) (2002) S163–S167.
[28] Y. Umebayashi, M. Honma, T. Abe, H. Ryuto, H. Suzuki, T. Shimazu, N. Ishioka, M. Iwaki, F. Yatagai, Mutation induction after low-dose carbon-ion beam irradiation of frozen human cultured cells, Biol. Sci. Space 19 (2005) 237–241.
[29] F. Yatagai, S. Morimoto, T. Kato, M. Honma, Further characterization of loss of heterozygosity enhanced by p53 abrogation in human lymphoblastoid TK6 cells: disappearance of endpoint hotspots, Mutat. Res. 560 (2004) 133–145.
[30] A.J. Grosvsky, B.N. Walter, C.R. Giver, DNA-sequence specificity of mutations at the human thymidine kinase locus, Mutat. Res. 289 (1993) 231–243.
[31] M. Honma, M. Izumi, M. Sakuraba, S. Tadokoro, H. Sakamoto, W. Wang, F. Yatagai, M. Hayashi, Deletion, rearrangement, and gene conversion; genetic consequences of chromosomal double-strand breaks in human cells, Environ. Mol. Mutagen. 42 (2003) 288–298.
[32] Y. Umebayashi, M. Honma, M. Suzuki, H. Suzuki, T. Shimazu, N. Ishioka, M. Iwaki, F. Yatagai, Mutation induction in cultured human cells after low-dose and low-dose-rate γ-ray irradiation: detection by LOH analysis, J. Radiat. Res. 48 (2006) 7–11.
[33] M. Inoue, G.-P. Shen, M.A. Chaudhry, H. Galick, J.O. Blaisdell, S.S. Wallace, Expression of the oxidative base excision repair enzymes is not induced in TK6 human lymphoblastoid cells after low doses of ionizing radiation, Radiat. Res. 161 (2004) 409–417.
[34] N. Yang, H. Galick, S.S. Wallace, Attempted base excision repair of ionizing radiation damage in human lymphoblastoid cells produces lethal and mutagenic double-strand breaks, DNA Repair 3 (2004) 1323–1334.
[35] P.J. Coates, S.A. Lorimore, E.G. Wright, Damaging and protective cell signaling in the untargeted effects of ionizing radiation, Mutat. Res. 568 (2004) 5–20.
[36] R. Iyer, B.E. Lehnert, Low-dose, low-LET ionizing radiation-induced radioadaptation and associated early responses in unirradiated cells, Mutat. Res. 503 (2002) 1–9.
[37] H. Matsumoto, A. Takahashi, T. Ohnishi, Radiation-induced adaptive and bystander effects, Biol. Sci. Space 18 (2004) 247–254.
[38] H. Matsumoto, A. Takahashi, T. Ohnishi, Nitric oxide radicals choreograph a radioadaptive response, Cancer Res. 67 (2007) 8574–8579.
[39] L.M. McLaughlin, B. Demple, Nitric oxide-induced apoptosis in lymphoblastoid and fibroblast cells dependent on the phosphorylation and activation of p53, Cancer Res. 65 (2005) 6097–6104.
[40] J.H. Yongblom, J.K. Wiencke, S. Wolf, Inhibition of the adaptive response of human lymphocytes to very low doses of ionizing radiation by the protein synthesis inhibitor cycloheximide, Mutat. Res. 227 (1989) 257–261.
[41] L.-H. Ding, M. Shingyoji, F. Chen, J.-J. Hwang, S. Burma, C. Lee, J.-F. Chen, D.J. Chen, Gene expression profiles of normal human fibroblasts after exposure to ionizing radiation: a comparative study of low and high doses, Radiat. Res. 164 (2005) 17–26.

Mutation Research 673 (2009) 9–20

Contents lists available at ScienceDirect

Mutation Research/Genetic Toxicology and Environmental Mutagenesis

journal homepage: www.elsevier.com/locate/gentox
Community address: www.elsevier.com/locate/mutres

Dose-dependent alterations in gene expression in mouse liver induced by diethylnitrosamine and ethylnitrosourea and determined by quantitative real-time PCR☆

Takashi Watanabe[a], Gotaro Tanaka[b], Shuichi Hamada[c], Chiaki Namiki[d], Takayoshi Suzuki[e], Madoka Nakajima[f], Chie Furihata[a,*]

[a] Functional Genomics Laboratory, School of Science and Engineering, Aoyama Gakuin University, Fuchinobe 5-10-1, Sagamihara, Kanagawa 229-0006, Japan
[b] Tokushima Research Center, Taiho Pharmaceutical Co. Ltd., Hiraishiebisuno 224-2, Kawauchichou, Tokushima, Tokushima 771-0194, Japan
[c] Genetic Toxicology Group, Toxicology Division II, Kashima Laboratory, Mitsubishi Chemical Safety Institute Ltd., Sunayama 14, Kamisu-shi, Ibaraki 314-0255, Japan
[d] Central Research Laboratory, SSP Co. Ltd., Nanpeidai 1143, Narita, Chiba 286-8511, Japan
[e] Division of Cellular & Gene Therapy Products, National Institute of Health Sciences, Kamiyoga 1-18-1 Setagaya-ku, Tokyo 158-8501, Japan
[f] Genetic Toxicology Group, Biosafety Research Center, Foods, Drugs, and Pesticides, Shioshinden 582-2, Fukude-cho, Iwata-gun, Shizuoka 437-1213, Japan

ARTICLE INFO

Article history:
Received 29 September 2008
Received in revised form 31 October 2008
Accepted 9 November 2008
Available online 21 November 2008

Keywords:
Genotoxic carcinogens
Dose-dependent alteration
Hierarchical clustering
k-means clustering
IPA

ABSTRACT

We examined the dose-dependency of gene expression changes for 51 genes in mouse liver treated with two *N*-nitroso genotoxic hepatocarcinogens, diethylnitrosamine (DEN) and ethylnitrosourea (ENU) by quantitative real-time PCR (qPCR). DEN (3, 9, 27 and 80 mg/kg bw) or ENU (6, 17, 50 and 150 mg/kg bw) was injected intraperitoneally into groups of five male 9-week-old B6C3F$_1$ mice and the livers were dissected after 4 h and 28 days. Total RNA from pooled livers was reverse-transcribed to cDNA and the amount of each gene was quantified by qPCR. Results were analyzed by hierarchical and *k*-means clustering and ingenuity pathway analysis (IPA). The most characteristic result was a similar dose-dependency of gene expression changes with DEN and ENU. Twenty-one genes exhibited a distinct dose-dependent increase in expression at 4 h for both carcinogens [*Bax*, *Btg2*, *Ccng1*, *Cdkn1a*, *Cyp4a10*, *Cyp21a1*, *Fos*, *Gadd45b*, *Gdf15*, *Hmox1*, *Hspb1*, *Isg20l1*, *Jun*, *Mbd1*, *Mdm2*, *Myc*, *Net1*, *Plk2*, *Ppp1r3c*, *Rcan1* and *Tubb2c*], although the increase in gene expression due to ENU was generally weaker than that due to DEN. Only *Gdf15* showed a dose-dependent increase in expression at 28 days for both carcinogens. The differences between DEN and ENU were in the expression of additional genes (7 for DEN and 8 for ENU). IPA extracted five gene networks: Network-1 included genes related to cancer and cell cycle arrest and associated with *Bax*, *Btg2*, *Ccng1*, *Cdkn1a*, *Gadd45b*, *Gdf15*, *Hspb1*, *Mdm2* and *Plk2* and Network-2 was related to DNA replication, recombination, repair and cell death and associated with *Cyp21a1*, *Gdf15*, *Ppp1r3c*, *Rcan1* and *Tubb2c*. The present results show a distinct dose-dependency of gene expression changes induced by DEN and ENU. These changes were associated with cancer, cell cycle arrest, DNA replication, recombination, repair and cell death and were seen not only at 4 h but also, for some, at 28 days after administration.

1. Introduction

Diethylnitrosamine (DEN) and ethylnitrosourea (ENU) are potent genotoxic *N*-nitroso carcinogens that induce hepatocellular carcinomas in mouse liver [1,2]. It has been reported that after its metabolic biotransformation, DEN produces the promutagenic adducts O^6-ethylguanine (O^6-EtG) and O^4- and O^2-ethylthymine and that O^4-ethylthymine may be responsible for the initiation of hepatocellular carcinomas in rats [3]. ENU, which is a direct-ethylating agent, forms several major adducts upon reaction with DNA, of which O^6-EtG, O^4- and O^2-ethylthymine and N^3-ethylthymine have been implicated in mutagenic lesions [4]. Suzuki et al. have reported that mutagenic activity by DEN and ENU was clearly detected with the *lacZ* mutation assay in mouse liver at 7 days [5]. Mientjes et al. have reported that the O^6-EtG levels increased as early as 1.5 h after treatment, whereas at 3 days more than 90% of the lesions had been removed from the DNA in the livers of DEN- and ENU-treated mice, based on *lacZ* transgenic mice [6]. After this period, however, with the bulk of O^6-EtG removed, the induction of *lacZ* mutations was observed at 3 days and continued to increase for some weeks.

☆ This work was a JEMS/MMS/Toxicogenomics group collaborative study.

* Corresponding author at: Department of Chemistry and Biological Science, School of Science and Engineering, Aoyama Gakuin University, 5-10-1 Fuchinobe, Sagamihara, Kanagawa 229-8558, Japan. Tel.: +42 759 6233; fax: +42 759 6511.
E-mail address: chiefurihata@gmail.com (C. Furihata).

1383-5718/$ – see front matter © 2008 Elsevier B.V. All rights reserved.
doi:10.1016/j.mrgentox.2008.11.004

Previously, Waring et al. showed by DNA microarray that a number of genes are up-regulated and down-regulated in rat liver, with rats dosed daily with DEN for 3 days and euthanized on the 4th day [7]. Genes up-regulated by DEN included genes related to growth arrest and DNA damage, such as *Bax*, *Ccnd1*, *Ccng1*, *Cdkn1a/p21*, *Gadd45* and *Jun*. However, no studies have focused on either the DNA damaging time of 4 h or the mutation fixing time of 28 days in DEN-treated mouse or rat liver. Although it has been reported that ENU induced expression of *Bax*, *Crp*, *Cyp2a*, *Gstm2*, *Icam1*, *Mig*, and *Mt2* mRNA in mouse liver, little is known about differential gene expression in ENU-exposed rodent liver [8].

Quantitative real-time PCR (qPCR) is an alternative technology for toxicogenomics [9]. qPCR is a highly regarded and reliable quantitative method but analysis of a large number of genes may be lengthy. It is impractical to examine a great number of genes with qPCR. Therefore, we selected 51 candidate genes (Table 1) based on our previous results using the Affymetrix GeneChip Mu74AV2 and original DNA microarray to determined the effects of DEN, dimethylnitrosamine, dipropylnitrosamine, ENU, *o*-aminoazotoluene, 7,12-dimethylbenz[*a*]anthracene, dibenzo[*a*,*l*]pyrene, phenobarbital and ethanol exposure in mouse liver for 4 and 20 h and 14 and 28 days in our JEMS/MMS/Toxicogenomics group collaborative study; results were reported in part [10]. We examined gene expression changes at an early time after administration, as we were interested in whether toxicogenomics was useful for carcinogen screening. In the previous study, using a single dose for each chemical, gene expression changes in number and degree were observed to peak at 4 h after administration. It is known that genotoxic *N*-nitroso carcinogens induce DNA damage and repair in a matter of a few hours after their administration; DNA adducts [6], DNA strand-breaks [11], unscheduled DNA synthesis [12] and other lesions have been reported. It is also known that mutations are observed in transgenic mouse liver 28 days after genotoxic *N*-nitroso carcinogen administration [5,6]. However, related gene expression changes at these time points have not yet been fully elucidated.

Table 1
Fifty-one genes examined in the present study.

No.	Symbol	Gene name	Accession number
1	*Bax*	Bcl2-associated X protein	NM_007527
2	*Bcl2*	B-cell leukemia/lymphoma 2	NM_009741
3	*Btg2*	B-cell translocation gene 2, anti-proliferative	NM_007570
4	*Casp1*	IL-1B converting enzyme; interleukin 1 beta-converting enzyme	NM_009807
5	*Ccnf*	Cyclin F	NM_007634
6	*Ccng1*	Cyclin G1	NM_009831
7	*Ccng2*	Cyclin G2	NM_007635
8	*Cdkn1a (p21)*	Cyclin-dependent kinase inhibitor 1A (P21)	NM_007669
9	*Cyp1a1*	Cytochrome P450, family 1, subfamily a, polypeptide 1	NM_009992
10	*Cyp1a2*	Cytochrome P450, family 1, subfamily a, polypeptide 2	NM_009993
11	*Cyp4a10*	Cytochrome P450, family 4, subfamily a, polypeptide 10	NM_010011
12	*Cyp21a1*	Cytochrome P450, family 21, subfamily a, polypeptide 1	NM_009995
13	*Dpyd*	Dihydropyrimidine dehydrogenase	NM_170778
14	*Egfr*	Epidermal growth factor receptor	NM_207655
15	*Ephx1*	Epoxide hydrolase 1, microsomal	NM_010145
16	*Fabp5*	Fatty acid binding protein 5, epidermal	NM_010634
17	*Fos*	FBJ osteosarcoma oncogene	NM_010234
18	*Gadd45b*	Growth arrest and DNA-damage-inducible 45 beta	NM_008655
19	*Gadd45g*	Growth arrest and DNA-damage-inducible 45 gamma	NM_011817
20	*Gapdh*	Glyceraldehyde-3-phosphate dehydrogenase	NM_008084
21	*Gdf15*	Growth differentiation factor 15	NM_011819
22	*Glul*	Glutamate-ammonia ligase (glutamine synthetase)	NM_008131
23	*Gstk1*	Glutathione S-transferase kappa 1	NM_029555
24	*Gyk*	Glycerol kinase	NM_212444
25	*Hist1h1c*	H1 histone family, member 2	NM_015786
26	*Hspa1b (Hsp70)*	Heat shock protein 1B	NM_010478
27	*Hspb1*	Heat shock protein 1	NM_013560
28	*Hspb2 (Hsp27)*	Heat shock protein 2	NM_024441
29	*Hmox1*	Heme oxygenase (decycling) 1	NM_010442
30	*Hprt1*	Hypoxanthine guanine phosphoribosyl transferase 1	NM_013556
31	*Igfbp1*	Insulin-like growth factor binding protein 1	NM_008341
32	*Isg20l1*	Interferon stimulated exonuclease gene 20-like 1	NM_026531
33	*Jun*	Jun oncogene	NM_010591
34	*Kras*	v-Ki-ras2 Kirsten rat sarcoma viral oncogene homolog	NM_021284
35	*Lig3*	Ligase III, DNA, ATP-dependent	NM_010716
36	*Lrp1*	Low density lipoprotein receptor-related protein 1	NM_008512
37	*Mbd1*	Methyl-CpG binding domain protein 1	NM_013594
38	*Mdm2*	Transformed mouse 3T3 cell double minute 2	NM_010786
39	*Myc*	Myelocytomatosis oncogene	NM_010849
40	*Net1*	Neuroepithelial cell transforming gene 1	NM_019671
41	*Pdgfb*	Platelet-derived growth factor, B polypeptide	NM_011057
42	*Plk2*	Polo-like kinase 2; serum-inducible kinase	NM_152804
43	*Pml*	Promyelocytic leukemia	NM_008884
44	*Pmm1*	Phosphomannomutase 1	NM_013872
45	*Ppp1r3c*	Protein phosphatase 1, regulatory (inhibitor) subunit 3C	NM_016854
46	*Rad52*	RAD52 homolog (S. cerevisiae)	NM_011236
47	*Rcan1(Dscr1)*	Regulator of calcineurin 1	NM_019466
48	*Trp53*	Transformation related protein 53	NM_011640
49	*Tubb2c*	Tubulin, beta 2c	NM_146116
50	*Ube2e1 (UbcM3)*	Ubiquitin-conjugating enzyme E2E 1, UBC4/5 homolog (yeast)	NM_009455
51	*Ung*	Uracil-DNA glycosylase	NM_011677

In this paper, we report our studies of gene expression changes in B6C3F$_1$ mouse liver induced by multiple doses of two typical alkylating agents, DEN and ENU. We investigated the dose-dependency of gene expression changes at two different time points: 4 h, characterized by the production of many DNA lesions, and 28 days, characterized by fixing of mutations [6]. If we could show dose-dependency in gene expression changes at 4 h, we could clarify key genes related to DNA lesions and subsequent various phenomena in liver cells induced by DEN and ENU. If we could show the dose-dependency in gene expression changes at 28 days, we could clarify key genes related to effects of mutations and subsequent changes that may be causal for carcinogenesis. Our purpose is to determine biological cell responses induced by DEN and ENU by examining the dose-dependency at these two time points.

In addition, we examined gene networks using IPA to elucidate interactions between genes with altered expression.

2. Materials and methods

2.1. Animal treatment

Male B6C3F$_1$ mice were obtained at 8 weeks of age from Charles River Japan, Inc. (Yokohama, Japan). They were kept in plastic cages on wood chips as bedding and given food (Oriental MF, Oriental Yeast Co., Tokyo) and water *ad libitum* in an air-conditioned room [12 h light (7 a.m. to 7 p.m.), 12 h dark; 23 ± 2 °C; 55 ± 5% humidity]. All animal experiments were conducted in accordance with the NIH Guide for Care and Use of Laboratory Animals and approved by the Animal Care and Use Committee at the Mitsubishi Chemical Safety Institute Ltd.

Mice at 9 weeks of age were injected intraperitoneally (i.p.) with DEN (3, 9, 27 and 80 mg/kg bw; Wako Pure Chem. Ind. Ltd., Osaka, Japan; CAS 55-18-5) dissolved in sterile water or ENU (6, 17, 50 and 150 mg/kg bw; Wako Pure Chem. Ind. Ltd., Osaka, Japan; CAS 759-73-9) dissolved in sterile water. Control animals for the DEN- and ENU-treated groups received sterile water. At 4 h and 28 days after treatment, animals were sacrificed after which the liver was collected, frozen on dry ice, and stored at −80 °C until use.

2.2. RNA isolation and relative quantification by real-time PCR

To isolate total RNA, approximately 150 mg from each liver (main lobe) was placed into TRIzol reagent (Invitrogen Corp., Carlsbad, CA, USA) and immediately homogenized using a Potter homogenizer. The samples were further homogenized with a 1 ml syringe and 18 gauge needle. Finally, total RNA was purified using an ethanol precipitation method. Complementary DNA (cDNA) was yielded from total RNA using the SuperScript First strand synthesis system for RT-PCR kit (Invitrogen Corp.).

qPCR amplifications were performed in triplicate using the SYBR Green I assay in an Opticon II (MJ Research, Inc., Waltham, MA, USA). The reactions were carried out in a 96-well plate in 20-μl reactions containing 2× SYBR Green Master Mix (Applied Biosystems, Lincoln Centre Drive Foster City, CA, USA), 2 pmol each of forward and reverse primer, and a cDNA template corresponding to 10 ng total RNA. Each primer sequence and Ct value are shown in Table 2. We selected 51 genes based on our previous results from the original DNA microarray and Affymetrix GeneChip Mu74AV2 for samples after treatment of DEN, dimethylnitrosamine, dipropylnitrosamine, ENU, *o*-aminoazotoluene, 7,12-dimethylbenz[*a*]anthracene, dibenzo[*a,l*]pyrene, phenobarbital and ethanol in our JEMS/MMS/Toxicogenomics group collaborative study. *Gapdh* and *Hprt1* were selected as housekeeping genes. SYBR Green PCR conditions were 95 °C for 10 min, followed by 95 °C for 10 s, 58 °C for 50 s and 72 °C for 20 s, for 45 cycles. In each assay a standard curve was determined concurrently with examined samples. In the preliminary experiment the highest group was selected for each gene and was used as the standard sample in the subsequent assay. In each standard curve determination, there were six dilution series of standard samples, diluted up to 1/5, 1/25, 1/125, 1/625 and 1/3125 of the selected standard liver cDNA for each gene. Finally, relative quantitative values of each sample were determined with 1/25 diluted cDNA and were normalized with those of the *Gapdh* genes. Relative *Gapdh* expression levels of experimental groups are presented in Fig. 1.

2.3. Data analysis and clustering algorithm

For the cluster analysis program, we performed a logarithmic ($\log_2$) transformation of the data to stabilize the variance and the gene expression profile of each DEN- and ENU-treated sample, normalized to the median gene expression level for the entire sample set. Both hierarchical and *k*-means clustering were performed using GENESIS software (http://genome.tugraz.at/) [13] for each data set at 4 h and 28 days separately. Gene groups were presented automatically by hierarchical clustering. Four clusters were set up initially in *k*-means clustering based on hierarchical clustering results. Genes which belonged to dose–response groups by both clustering methods were defined as dose–response genes. Furthermore, genes which showed less than a 0.5-fold decrease dose-dependently were evaluated as decrease genes by expression pattern because the decrease genes were few and could not be extracted using both clustering methods.

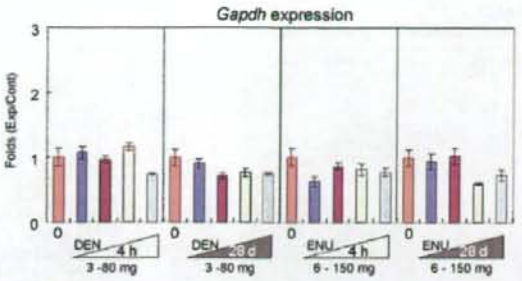

Fig. 1. Relative expression of *Gapdh*. DEN (0–80 mg/kg bw) and ENU (0–150 mg/kg bw) were given to 9-week-old mice (five per group). Total RNA was extracted from pooled liver and reverse-transcribed to cDNA. *Gapdh* expression was determined by qPCR in triplicate assays. Results are shown as mean ± S.D.

The color displays given in Fig. 2 show the $\log_2$ (expression ratio) as (1) red when the treatment sample is up-regulated relative to the control sample, (2) blue when the treatment sample is down-regulated relative to the control sample and (3) white when the $\log_2$ (expression ratio) is close to zero.

2.4. Pathway analysis

Numerical experimental data at 4 h and 28 days after DEN or ENU treatment were separately analyzed by ingenuity pathway analysis (IPA) Software-Complete Pathways Database. These data were generated through the use of IPA, a web-delivered application (www.Ingenuity.com) that enables the visualization and analysis of biologically relevant networks to discover, visualize, and explore therapeutically relevant networks. IPA information was extracted by experts from the full text of the scientific literature, including information about genes, drugs, chemicals, cellular and disease processes, and signaling and metabolic pathways.

Expression data sets containing gene identifiers (Entrez gene identifiers) and their corresponding expression values as fold changes were uploaded as a tab-delimited text file. Each gene identifier was mapped to its corresponding gene object in the Ingenuity Pathways Knowledge Base. To start building networks, the application program queries the Ingenuity Pathways Knowledge Base for interactions between focus genes and all other gene objects stored in the knowledge base and generates a set of networks. The program then computes a score for each network according to the fit of the network to the set of focus genes. The score indicates the likelihood of the focus genes in a given network being found together due to random chance. A score of >2 indicates that there is a <1 in 100 chance that the focus genes were assembled randomly into a network due to random chance.

3. Results

3.1. Dose-dependent alteration of gene expression induced by DEN

3.1.1. Clustering analysis for gene expression

Unsupervised hierarchical clustering results are shown in Fig. 2. The changes in gene expression are represented colorimetrically as described in Section 2. The clustering presented four groups (DEN-4 h-Grp-1 to DEN-4 h-Grp-4) and an ungrouped gene 4 h after administration, and three groups (DEN-28 d-Grp-1 to DEN-28 d-Grp-3) and eight ungrouped genes 28 days after administration. As unsupervised hierarchical clustering was performed for 4 h and 28-day samples separately, group member genes were different for 4 h groups and 28-day groups.

At 4 h, all 20 DEN-4 h-Grp-1 genes showed a dose-dependent increase of more than 3–64-fold. Twelve DEN-4 h-Grp-2 genes were suggested to have a gradual dose-dependent increase of less than that for the expression in DEN-4 h-Grp-1. Two DEN-4 h-Grp-4 genes exhibited a dose-dependent decrease of less than 0.3-fold.